

Seeding of breast cancer cell line (MDA-MB-231^{LUC+}) to the mandible induces overexpression of substance P and CGRP throughout the trigeminal ganglion and widespread peripheral sensory neuropathy throughout all three of its divisions

Molecular Pain
Volume 17: 1–17
© The Author(s) 2021
Article reuse guidelines:
sagepub.com/journals-permissions
DOI: 10.1177/17448069211024082
journals.sagepub.com/home/mpx


Silvia Gutierrez¹, James C Eisenach¹, and M Danilo Boada¹ 

Abstract

Some types of cancer are commonly associated with intense pain even at the early stages of the disease. The mandible is particularly vulnerable to metastasis from breast cancer, and this process has been studied using a bioluminescent human breast cancer cell line (MDA-MB-231^{LUC+}). Using this cell line and anatomic and neurophysiologic methods in the trigeminal ganglion (TG), we examined the impact of cancer seeding in the mandible on behavioral evidence of hypersensitivity and on trigeminal sensory neurons. Growth of cancer cells seeded to the mandible after arterial injection of the breast cancer cell line in Foxn1 animals (allogeneic model) induced behavioral hypersensitivity to mechanical stimulation of the whisker pad and desensitization of tactile and sensitization of nociceptive mechanically sensitive afferents. These changes were not restricted to the site of metastasis but extended to sensory afferents in all three divisions of the TG, accompanied by widespread overexpression of substance P and CGRP in neurons through the ganglion. Subcutaneous injection of supernatant from the MDA-MB-231^{LUC+} cell culture in normal animals mimicked some of the changes in mechanically responsive afferents observed with mandibular metastasis. We conclude that released products from these cancer cells in the mandible are critical for the development of cancer-induced pain and that the overall response of the system greatly surpasses these local effects, consistent with the widespread distribution of pain in patients. The mechanisms of neuronal plasticity likely occur in the TG itself and are not restricted to afferents exposed to the metastatic cancer microenvironment.

Keywords

Cancer, pain, nociception, sensitization, MDA-MB-231^{LUC+}, SP, CGRP

Date Received: 18 March 2021; Revised 19 May 2021; accepted: 19 May 2021

Introduction

The peripheral nervous system is known to regulate organ homeostasis. Particularly important to this process after injury or disease is the local activation of nociceptive sensory afferents (peripheral pain sensors), which release peptides into surrounding tissues, resulting in neurogenic inflammation. Overall, this process has two direct consequences: local immuno-modulation important to tissue repair and central transmission resulting in pain and noci-defensive behaviors to avoid further damage. These peripheral nociceptive responses may be activated by metastatic cancer due to mechanical

disruption of nerves, local ischemia, inflammation, or secreted products from cancer cells themselves.¹

In this manner, pain experienced by patients in some forms of aggressive cancer may be related to disease progression and poor prognosis.² In most cases, this

¹Wake Forest Baptist Medical Center, Winston-Salem, NC, USA

Corresponding Author:

M Danilo Boada, Wake Forest University Baptist Medical Center, 1 Medical Center Blvd., Winston-Salem, NC 27103, USA.

Email: mboada@wakehealth.edu



pain cannot be explained by the magnitude of tissue damage or the local inflammatory process, indicating a neuropathic nature.^{1,3-6} In head and neck cancer, including metastatic cancer to the mandible,⁷⁻¹⁰ symptoms ranging from trigeminal neuralgia to persistent idiopathic unilateral facial pain and sensory loss can be the hallmark of widespread metastases beyond the head and neck.¹¹⁻¹⁴

Due to the unique anatomy of the trigeminal ganglion (TG: multiple major branches converging in a single structure), the study of orofacial pain syndromes is particularly challenging. Current surgical and oncological models largely concentrate on the effects of nerve damage to one of the individual TG branches, usually by transection or ligation of the infraorbital nerve¹⁵⁻¹⁷ or cancer implanted in the tongue,¹⁸ lower gum,¹⁹ or whisker-pad.²⁰ The degree to which these models mimic specific features of the patient's symptomatology is frequently not satisfactory.²¹ In general, these studies restrict examination to the local area innervated by the injury and do not assess the potential for a widespread sensitization process beyond the injured trigeminal division.

Furthermore, the trigeminal ganglia (TG) nociceptive network has multiple cellular components and is not homogenous. The network's density, modality, properties, and responsiveness to injury not only depend on specific neuronal subtypes but also on the unique tissue and organs innervated.^{22,23} This explains why histologically different cancers involving disparate anatomic sites produce a different pain phenotype.^{24,25}

In this context, pain caused by metastatic cancer to the bone is unique in severity. Although clearly associated with the function of this bone and tensile-elastic properties, nociceptive bone innervation is particularly prone to cancer activation. The relationships between bone nociceptive innervation-specific cellular subtypes and their vulnerability to cancer-mediated activation are essential to understanding their contribution to the early stages of the disease.

In addition to the local sensitization produced by physical cancer growth, stimulation of the V3 division of the TG has been observed to result in transganglionic activation, leading to upregulation of both mitogen-activated protein kinase (MAPK) and inflammatory proteins in regions of the TG associated with all 3 divisions TG.^{26,27} Orofacial pain develops early in carcinogenesis and worsens with disease progression.^{25,28} Onset of pain has been associated with the transition of oral precancer to cancer.³ Several molecules released by cancer cells can activate peripheral sensory afferent terminals, resulting in pain and local neuro-inflammation.^{29,30} From a neurobiological standpoint, metastatic cancer to bone is also unique. Metastatic cancer cells express receptors to several neurokinins

that are locally released by activated nociceptors, and stimulation of these neurokinin receptors on cancer cells has been implicated in a myriad of processes related to oncogeneses such as mitogenesis, angiogenesis, cell migration, and metastasis.³¹⁻³⁴

The bioluminescent human breast cancer cell line MDA-MB-231^{LUC+} is extremely unique and valuable to study cancer-induced facial pain due to its natural propensity to invade the left mandible after intracardiac injection and to express luciferase, allowing the assessment of tumor implantation at early stages of the tumor progression.³⁵ Due to its sex-specific origin, no attempt has been made to demonstrate its potential to be used in male animals to isolate potential sex influences on the development of cancer-induced facial pain at early stages. In addition, this cell line also expresses these neurokinin receptors, including those to substance P (SP) and calcitonin gene-related peptide (CGRP), which participate in rapid cancer growth.³⁶⁻³⁸ Although these data suggest that tumor growth globally modifies afferent sensibility throughout the trigeminal system, no neurophysiological evidence has demonstrated this assumption.

The current study aims to fill this gap in our knowledge on the feasibility of the use of MDA-MB-231^{LUC+} in male animals. We will also clarify the sensory effects of mandibular seeding of MDA-MB-231^{LUC+} cells by evaluating behavioral, neurophysiological, and anatomical consequences during metastatic tumor growth. Based on the available cited literature¹⁵⁻²⁰ and our own observations in other local injury models,^{38,39} we hypothesized that these sensory effects (nociceptive mechanical sensitization) should be restricted to the affected area by the seeding (mandible, V3 branch). We further test the relevance of factors released by these cancer cells on trigeminal sensory afferents by subcutaneous injection of the supernatant of cell line culture in the receptive field of afferents in normal animals.

Methods

Animals

Forty male mice aged 4–6 weeks of age (The Jackson Laboratory, Bar Harbor, ME, USA) were studied in one of two experiments (Figure 1(a)). The first examined the effects of cancer seeding the mandible and was performed in 20 B6.Cg *Foxn1*^{tm/J} (*Foxn1*) immunodeficient mice. The second study examined the acute effects of injection of cell-free supernatant from cancer cell culture into the receptive fields of recorded afferents in 20 C57BL/6J mice, termed wild type (WT). In both studies, mice were housed in pairs in a climate-controlled room under a 12-h light/dark cycle. The use and handling of animals were in accordance with guidelines provided by

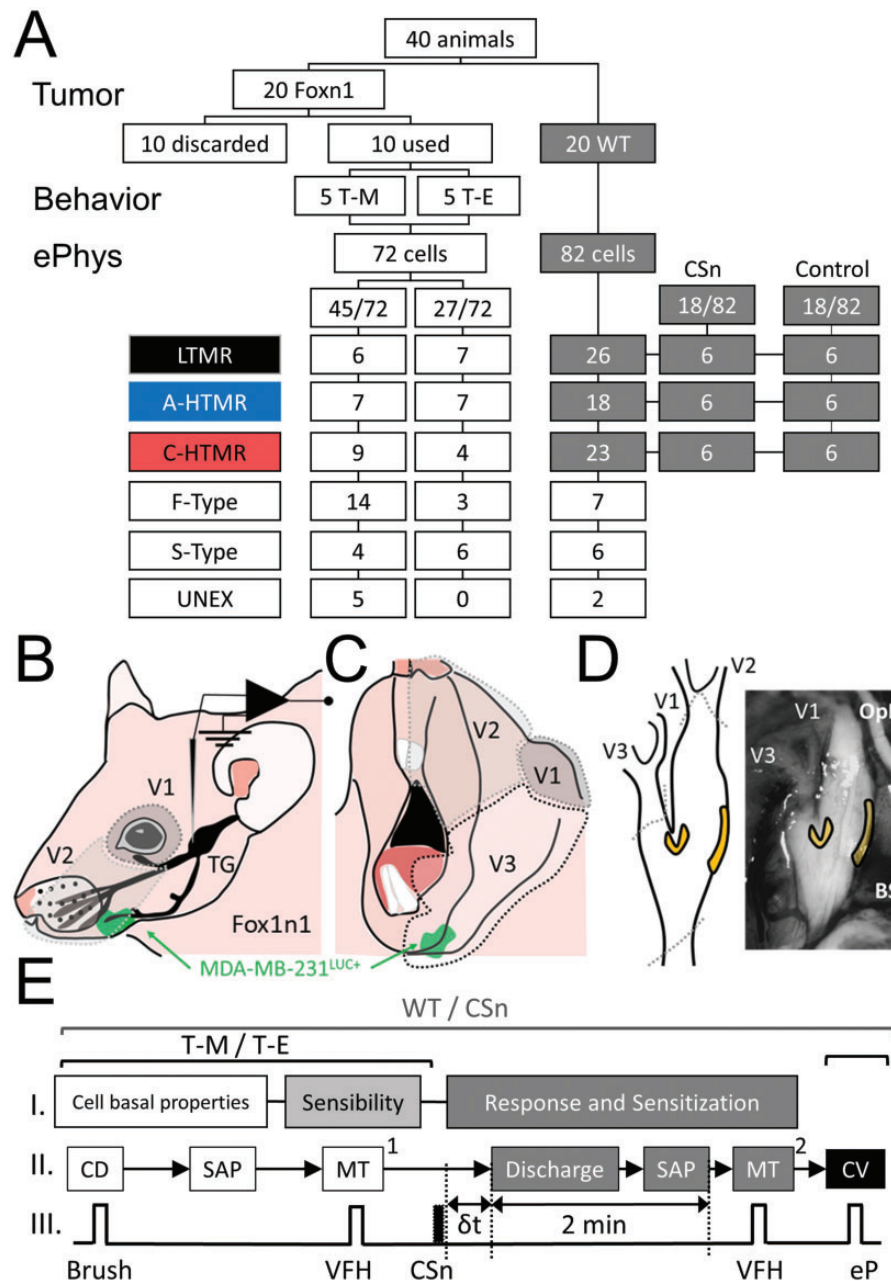


Figure 1. (a) Flowchart, procedures, and classification of the neurons included in the study in wild type (WT: C57BL/6) and Foxn1 (B6.Cg-Foxn1^{nu/nu}) mice with MDA-MB-231^{LUC+} tumor in the left mandible (**T-M**) or elsewhere than the head and neck region (**T-E**). Neurons were classified by subtype: LTMR: low threshold mechanoreceptors, A-HTMR: A fiber high threshold mechanoreceptor, C-HTMR: C fiber high threshold mechanoreceptor, F-Type: fast action potential (AP) dynamic mechanically unresponsive, S-Type: slow AP dynamic mechanically unresponsive, UNEX: electrically unexcitable cells. (b) Lateral-upper view of the innervation territories of the V1 and V2 divisions of the trigeminal nerve and location of the trigeminal ganglion (TG). (c) Lateral-lower view of the innervation territory of the V3 division of the trigeminal nerve. (d) Locations within the TG where the recordings were performed (yellow). Dotted gray areas (a and b) represent the likelihood of innervation by specific TG branches (V1: ophthalmic nerve; V2: maxillary nerve; V3: mandibular nerve). The green area represents the approximate relative location of the tumor (MDA-MB-231^{LUC+}) with respect to the TG innervation areas. OpN: optic nerve. BS: brain stem. (e) Sequence of electrophysiological recordings in the study of subcutaneous injection of the supernatant of cell cultures of MDA-MB-231^{LUC+} cells in Wild Type mice (WT/CSn) and foxn1 mice with MDA-MB-231^{LUC+} tumors in the mandible or elsewhere beyond the head and neck (T-M/T-E). In all cases cellular baseline properties including receptive field (RF) area and somatic active electrical properties (SAP) obtained during RF characterization occurred first, followed by determining mechanical sensibility by measuring the mechanical stimulation [MT¹] in response to von Frey hair (VFH) application, and in all cases, the last measurement was that of conduction velocity (CV) using an electrical pulse (eP). In the WT/CSn, the time from subcutaneous (s.c.) injection and spontaneous discharge (δt) of HTMRs was recorded, and SAP of these action potentials was measured during a 2 min observation period. Mechanical threshold at the end of these 2 minutes was measured.

the National Institutes of Health and the International Association for the Study of Pain, and all procedures and experiments were approved by the Institutional Animal Care and Use Committee of Wake Forest University Health Sciences.

Cancer cell line selection, culture, and implantation

We selected the human mammary cancer cell line (MDA-MB-231^{LUC+}) because of its distinct organ-specific metastatic potential,⁴⁰ proclivity to seed in the mandible of mice after intracardiac injection (thereby eliminating the need to inoculate the bone and induce collateral damage), and its bioluminescent signal that allows tumor detection and non-invasive structural evaluation *in vivo*.³⁵ The latter two aspects are of critical importance for the appropriate evaluation of the effects of a mandible cancer xenograft model on TG afferents.

a. *Cell culture, reagents, and treatments.* MDA-MB-231^{LUC+} cells that stably express firefly luciferase gene (#AKR-231, Cell Biolabs, CA, US) were grown at 37°C and 5% CO₂ in DMEM media (#11995-065, Gibco by Life Technologies, NY, US), containing MEM Non-Essential Amino Acids (#11140-050, Thermo Fisher Scientific, MA, US), 10% fetal bovine serum (FBS) (#F2442, Sigma, MO, US), penicillin/streptomycin (#15140-122, Gibco by Life Technologies, NY, US) and amphotericin B (#400-104, Gemini Bio-products, Ca, US). No peptidase inhibitor was used. After the cells reached confluence, cell culture media was replaced with FBS-free cell culture media, and cells were incubated on it for 72 hours prior to supernatant collection.⁴¹ FBS-free cell culture supernatants from MDA-MB-231^{LUC+} (CSn) and FBS-free cell culture media (control) were collected fresh prior to electrophysiological experiments and diluted 1:1 with artificial cerebrospinal fluid (aCSF [in mM]: 127.0 NaCl, 1.9 KCl, 1.2 KH₂PO₄, 1.3 MgSO₄, 2.4 CaCl₂, 26.0 NaHCO₃, and 10.0 D-glucose). In these experiments, selected cells from WT animals were identified and characterized (see Cellular Classification Protocol), and then 5 ml of subcutaneous CSn or control solution were injected within their receptive fields (RFs).

b. *Cell line implantation.* Seeding of MDA-MB-231^{LUC+} cells to the mandible after intracardiac injection was performed as described elsewhere.³⁵ Briefly, cultured cells were rapidly (< 2 min) injected into the left ventricle of 20 Foxn1 mice (100 µl, 1 × 10⁶ cells diluted in Hank's balanced salt solution [HBSS]),³⁵ and the presence and growth of MDA-MB-231^{LUC+} cells in the neck, mandible, other cranial bone, thoracic cavity, and limbs were tracked through bioluminescence (once per week) imaging using an IVIS Imaging

System with X-ray capabilities (IVIS Lumina In Vivo Imaging System, USA). This information was used only to corroborate the presence and location of the tumors but not their growth. Three weeks after injection, animals with a tumor in the left mandible (T-mandible [T-M]) and those with tumors outside the trigeminal domain (T-elsewhere [T-E]) were prepared for the electrophysiologic study of TG afferents. Following the electrophysiologic study, animals were perfused intracardially with fixative, and the TGs and both mandibles were removed for immunohistochemistry (see below). Animals that showed no bioluminescence evidence of tumors two weeks after left ventricular injection were euthanized and not included in the study.

Behavioral tests

Behavioral assessment was performed in animals in the tumor seeding study on the day before the electrophysiologic study. For mechanical withdrawal threshold assessment, mice were placed in a plastic cage and acclimatized to the environment for at least 30 min prior to testing. Withdrawal threshold was determined by applying calibrated von Frey filaments (0.41, 0.70, 1.20, 2.00, 3.63, 5.50, 8.50, and 15.10 g) (Stoelting, Wood Dale, IL, USA) to the left facial pad (vibrissa pad) of the animals. A response was considered positive if the animal rapidly withdrew the head or when flinching was observed after the stimulation. To reduce bias, this behavioral measurement was performed by an observer who was blinded to the group, as neither T-mandible nor T-elsewhere animals showed external signs of tumor or exhibited spontaneous behaviors related to tumor presence.

Electrophysiology

Animals were deeply anesthetized with isoflurane (initial inhaled concentration 3%, Teva Pharmaceuticals, North Wales, PA), the trachea intubated, and lungs ventilated using pressure-controlled ventilation (Inspira PCV, Harvard Apparatus, Holliston, MA) with humidified oxygen. Heart rate and noninvasive blood pressure were monitored throughout as a guide to the depth of anesthesia. Inspired end-tidal isoflurane concentration was maintained at 2% throughout the study and adjusted prior to removal of the cortex based on heart rate and blood pressure. For animals in the CSn experiments, the hair over the left side of the face was clipped. In all animals, a craniotomy was performed, the brain tissue frontal to the cerebellar tentorium was surgically removed, and the exposed tissues covered with gelatin foam. The skull cavity was continuously perfused with oxygenated aCSF. The animal was secured using custom stainless-steel clamps and transferred to a preheated

(32–34°C) recording chamber where the superfusate temperature was slowly raised to $37 \pm 0.2^\circ\text{C}$ using an infusion pump (MPRE8, Cell MicroControls, Norfolk, VA). Pool temperature adjacent to the TG was monitored with a thermocouple (IT-23, Physitemp, Clifton, NJ). Rectal temperature (RET-3, Physitemp) was maintained at $34 \pm 1^\circ\text{C}$ with radiant heat.

The total period of electrophysiological recording was limited to a maximum of 75 min in order to diminish the likelihood that experimental manipulation would result in afferent sensitization. TG neuronal somata were impaled with quartz micropipettes (80–250 M Ω) containing 1 M potassium acetate. Direct current output from an Axoclamp 2B amplifier (Axon Instruments/Molecular Devices, Sunnyvale, CA) was digitized and analyzed off-line using Spike2 (CED, Cambridge, UK). The sampling rate for intracellular recordings was 21 kHz throughout (MicroPower1401, CED).

Cellular classification protocol

The general procedure to classify primary sensory afferents was applied as described elsewhere for dorsal root ganglia⁴² and the TG.²³ The receptive field (RF) was searched, starting on the lower mandible in a lateral pattern, first covering the oral cavity and then progressing to the mandible hairy skin cephalad to the maxilla and forehead and ending 5 mm below the surgical incision. Neurons with RF located near the nose clamp or the skin incision were excluded because of the potential sensitization of those afferents. RFs were located with the aid of a stereomicroscope using increasing mechanical stimulation; the latter progressed from light touch with a fine sable hair paintbrush to searching with a blunt probe (back of the paintbrush) and ultimately gentle to strong pinching with fine-tipped forceps. In every case, the cellular RF and neuronal soma position relative to the innervating branch (V1/V2 or V3) were noted for post hoc analysis (Figure 1(b) to (d)). Although in some cases cells innervating V1 and V2 were identifiable by their location and mechanical thresholds (e.g., eyelid area vs. whisker pads, see results), we decided to combine the information of afferents in both areas (V1/V2) due to the potential degree of overlapping of their innervation and the uncertainty of their branching origin. No attempt to further classify cells innervating specific hair structures was performed due to the differences between strains (Foxn1 are nude).

a. *Cells with RF*: Based on the combination of their mechanical threshold, conduction velocity (CV), and dynamic response (phasic; on-off; tonic), neurons were classified into three groups: LTMRs (low-threshold mechanoreceptors, rapidly adapting [RA] tactile afferents), AHTMRs (A fiber high-threshold

mechanoreceptors), and CHTMRs (C fiber high-threshold mechanoreceptor) innervating facial skin. Specific cellular subtypes such as slowly adapting (SAI and SAII)⁴³ tactile afferent neurons (tactiles with a low percentage [13.1%] of stable impalement in the TG),²³ C-polymodal nociceptor (nociceptors which saturate their responses well below the mechanical nociceptive thresholds in humans),^{44–47} muscle spindles (MS) and cells innervating specialized structures (cornea, internal oral cavity, teeth)²³ were not studied.

b. *Cells without RF*: Cells that were electrically excitable but without mechanical RF were separated into two different populations based on the shape of the action potential (AP)^{42,48–50} as neurons with inflection in the repolarizing phase (slow, or S-type neurons) and neurons without this inflection (fast, or F-type neurons). To more clearly determine the presence of this inflection, the first derivative records of the AP were used (presence or absence of a second additional negative component in the time course of the AP first derivative). Cells without RF or electrical excitability were classified as unexcitable (UNEX). Since RF properties, especially response characteristics, were used to define differences in the fast-conducting afferents (those without inflected APs), the ability to accurately define and categorize these three populations further was not possible. After electrical characterization, S-type, F-type, and UNEX cells were included in the description of distribution but not otherwise examined.

All included cells satisfied the following requirements: Resting membrane potential (E_m) more negative than -40 mV, AP amplitude ≥ 30 mV, and the presence of afterhyperpolarization (AHP). Passive membrane properties indicative of poor impalement (extremely low input resistance [R $_i$] and extremely short time constant [τ , τ]) were also reasons for exclusion. Fiber conduction velocity (CV) was always measured at the end of the recording.

Mechanical sensitivity and cellular excitability

Peripheral and somatic cellular excitability was measured at three stages (Figure 1(e)). All groups included: (1) Cellular basal properties (CBP) and (2) mechanical sensibility. In the second experiment, effects of cancer supernatant on changes in CBP, spontaneous activity, and sensitization to mechanical stimulation were also examined.

1. Cellular basal properties: This protocol applied to all groups (T-M, T-E, and WT CSn) and included RF

area mapping, somatic active electrical properties, and afferent CV (Figure 1(e)-I):

- a. **RF area mapping:** After identifying the cellular RF area of responsiveness to the search stimuli, the area was marked using a red fine point marker. This initial procedure was performed gently to avoid damaging the skin (as assessed visually by lack of development of erythema, edema, glossiness, etc.).
- b. **Somatic Active Electrical Properties:** Active membrane properties of all excitable neurons were analyzed in APs obtained during RF characterization. These parameters included amplitude and duration of the AP and AHP of the AP, along with the maximum spike depolarization rate (MDR) and repolarization rate (MRR). AP and AHP durations were measured at half-amplitude (D50 and AHP50, respectively) to minimize hyperpolarization-related artifacts.
2. **Mechanical Sensibility:** Resting mechanical threshold (MT^1) was determined in each afferent with calibrated von Frey filaments (Stoelting, Wood Dale, IL) as the minimum force to generate at least one AP, testing the most sensitive area of the cellular RF. The presence or absence of post-discharge hyperpolarization (PDH)⁵¹ was determined during this procedure.
3. **Response and sensitization (CSn study only):** Response was defined as the change in the normal cellular response and the time (δt , sec) from CSn or control application to this change. For LTMRs, the modification was a change in response to mechanical threshold stimulation, whereas, for HTMRs, it was spontaneous discharge without mechanical stimulation. The spontaneous discharge was characterized as the number of APs, the maximal instantaneous frequency [IF max, Hz], D50, AHP, and AHP as compared to the period prior to CSn or control application.

Sensitization was defined as the change in the mechanical threshold of nociceptive afferents after study media application. This threshold (MT^2) was tested 2 min after media application and compared to the baseline threshold (MT^1) (Figure 1(e)-II and III).

Conduction Velocity. Spike latency was obtained by stimulating the RF at the skin surface using a bipolar electrode (0.5 Hz, current range: 0.1–1.2 mA) and a stimulus isolator (A360LA, WPI, Sarasota, FL, USA). This was performed following mechanical stimulation to prevent potential alterations in RF properties by electrical stimulation. All measurements were obtained using the absolute minimum intensity required to excite neurons consistently without jitter. This variability (jitter) in the AP generation latency, particularly at significantly shorter latencies seen at two- to three-fold threshold

intensity, has been presumed to reflect spread to more proximal sites along axons. Stimuli ranged in duration from 50 to 100 μ s; utilization time was not taken into account. The distance was measured for each afferent on termination of the experiment by inserting a pin through the RF (marked with ink at the time of recording) and carefully measuring the distance to the TG along the closest nerve (Figure 1(e)-III).

Immunohistochemistry

Tissue preparation. Following the electrophysiological experiments, the thorax was opened, and fixative (4% paraformaldehyde in 0.1 M phosphate buffer, pH 7.4) was perfused through the left ventricle with a peristaltic pump at 20 ml/min for 15 min. Ipsilateral and contralateral TG and jawbones were then identified, removed, and immersed in fixative for 2 h at 4°C. Afterward, the ganglia and jawbones were washed with 0.01M phosphate buffer saline (PBS). Jawbones were decalcified in 10% EDTA (#60-004, Sigma, St Louis, MO, USA) for two weeks at 4°C until it reached complete demineralization. Afterward, the TG and jawbones were then immersed in 30% sucrose at 4°C for cryoprotection until sectioned on a cryostat. Sections (18 μ m) were collected on slides and stored at –80°C until processed. TG sections from 3 animals (contralateral and ipsilateral) were processed simultaneously using antibodies against substance P (SP) and calcitonin gene-related peptide (CGRP) as follows. Sections were washed with PBS with 0.1% Triton X-100 (PBST), incubated one hour in blocking solution (1.5% normal donkey serum (# 017-000-121, Jackson Immuno Research Labs, West Grove, PA, USA) in PBST and overnight at 4°C with the following primary antibodies: rat anti-SP (1:500, #556312, BD Biosciences, San Jose, CA, USA) and rabbit anti-CGRP (1:10 000, #C8198, Sigma, St Louis, MO, USA). Jawbone sections were reacted with goat anti-Luciferase antibody (1:2000, #NB100-1677, Novus, Centennial, CO, USA). Subsequently, sections were washed three times for ten minutes with PBS and incubated for 2 h at room temperature with the corresponding secondary antibodies: donkey anti-rat Cyanine 2 (1:400) and anti-rabbit Cyanine 3 (1:500) or donkey anti-goat Cyanine 5 (1:400) (Jackson Immuno Research Labs, West Grove, PA, USA). Finally, jawbone sections were reacted with DAPI (1:10000, # D21490, Invitrogen). All sections were then washed thoroughly in PBS, mounted on plus-slides, air-dried, dehydrated in ethanol, cleared in xylene, and coverslipped with DPX mounting media (Sigma-Aldrich, MilliporeSigma, St. Louis, MO, USA).

SP antibody specificity was tested in tachykinin knock-out mice.⁵² There is no commercially available blocking peptide for rabbit anti-CGRP (# C8198,

Sigma, St Louis, MO, USA), although this antibody is being previously used in mouse tissue.^{52,53} SP and CGRP antibody specificity were also verified by deletion of the primary antibody (data not shown).

Image acquisition and analysis

Images from three to five randomly selected sections ipsi- and contra-lateral to the mandibular tumor were captured with a CCD digital camera attached to a Nikon E600 epifluorescence microscope with a 20× objective. Images obtained were coded, so the experimenter performing image analysis was blinded to the group. The intensity of immunostaining to SP or CGRP was quantified automatically using Image J (U. S. National Institutes of Health, Bethesda, Maryland, USA, <http://imagej.nih.gov/ij/>, 1997–2011) as previously described.³⁸ Quantification for each image was performed, calculating the average from three to five randomly selected TG sections per mouse. The numbers of pixels occupied by immunoreactive cells with intensity above a fixed threshold (used for the analysis of all sections) and within the defined area (pixels/mm²) was conducted automatically with integrated density (sums all of the pixels within a region). The average was then calculated per animal and per group.

Statistical analysis

Before analysis, parametric assumptions were evaluated for all variables using histograms, identifying outliers with boxplots, descriptive statistics, and the Shapiro–Wilk test for normality. Data are reported as median (range or quartiles) if not normally distributed or mean (standard error) if normally distributed. Student's t-test and repeated measures analysis of variance (ANOVA) were used for normally distributed data, and Friedman test and Mann Whitney U-test were used for not normally distributed data. Changes in Em in AHTMR over time were analyzed using repeated-measures ANOVA with Greenhouse & Geisser sphericity correction as distributions at each time point proved to be parametric, and there were no significant outliers. Friedman tests were run on the number of APs per stimuli and duration data as the distributions were non-parametric at one or more time points in each dependent variable. For all analyses, p was set at 0.05 for statistical significance. All post-hoc analyses were Bonferroni adjusted. Analyses were carried out using SPSS Statistics for Windows, version 22 (IBM Corp, Armonk, NY), and OriginPro 9.5 (Northampton, MA).

Results

Figure 1(a) depicts the animal disposition and cell types recorded in the two experiments. In the first experiment,

two weeks after intracardiac injection of MDA-MB-231^{LUC+} five of the 20 Foxn1 mice developed bioluminescent evidence of tumor seeding in the left mandible (**T-M**), five demonstrated no evidence of tumor, and 10 demonstrated tumor outside the head-and-neck region (**T-E**). One week later, electrophysiologic recordings were made in the 5 **T-M** animals and 5 of the **T-E** animals. In the second experiment, 20 C57BL/6J mice were used to collect information on afferents of these control animals (**WT**) (82 cells) to be compared with **T-M** (45 cells) and **T-E** (27 cells) and to further evaluate the effects of the CSn (obtained from MDA-MB-231^{LUC+} cultured cells) on the sensibility and responsiveness of TG mechanosensory afferents (6 per type, 18 CSn vs control, 36 cells).

Mandibular metastasis and facial withdrawal threshold: Figure 2(a) to (c) shows the typical bioluminescence in the animals with mandibular cancer, three weeks after intracardiac injection of MDA-MB-231^{LUC+} cells, prior the electrophysiologic study. Clear bioluminescence above 1400 counts (Figure 2(a)) overlapped the lower left jawbone structure (Figure 2(b)) in these animals. Gross and histologic analysis corroborated the presence of a lesion on the anterior portion of the animal's left incisor at the labial dental epithelium region (Figure 2(c) and (d)). Lower facial withdrawal threshold was significantly decreased in **T-M** compared to **T-E** animals (Figure 2(e); $p < 0.001$).

Electrophysiology

Cellular basal properties.

- Cellular Distribution (CD):* The distribution of cells recorded and analyzed by group in the study is diagrammed in Figure 2(f) and detailed in the text below. Of note, approximately two-thirds of cells were mechano-sensitive in WT (82%) and Foxn1 **T-E** (67%) animals, compared to approximately half (49%) in **T-M** animals, although this difference was not statistically significant.
- Somatic active electrical properties (SAP).* As shown in Table 1, some characteristics of the generated *spike* are distinctly preserved between different types of mechanosensory afferents. In all three groups LTMR afferents, have a significantly smaller amplitude and shorter duration than nociceptive afferents ($p < 0.05$ and $p < 0.01$ vs A- and CHTMRs, respectively). In WT animals, spike depolarization (MDR) and repolarization (MRR) rates in LTMRs, exhibited faster spike kinetics ($p < 0.05$) than C but not AHTMRs. Although this difference between APs kinetics is maintained in **T-E** animals, it completely disappears in **T-M** animals as a consequence of a significant reduction in the MDR ($p < 0.05$) and MRR ($p < 0.01$) of LTMR afferents.

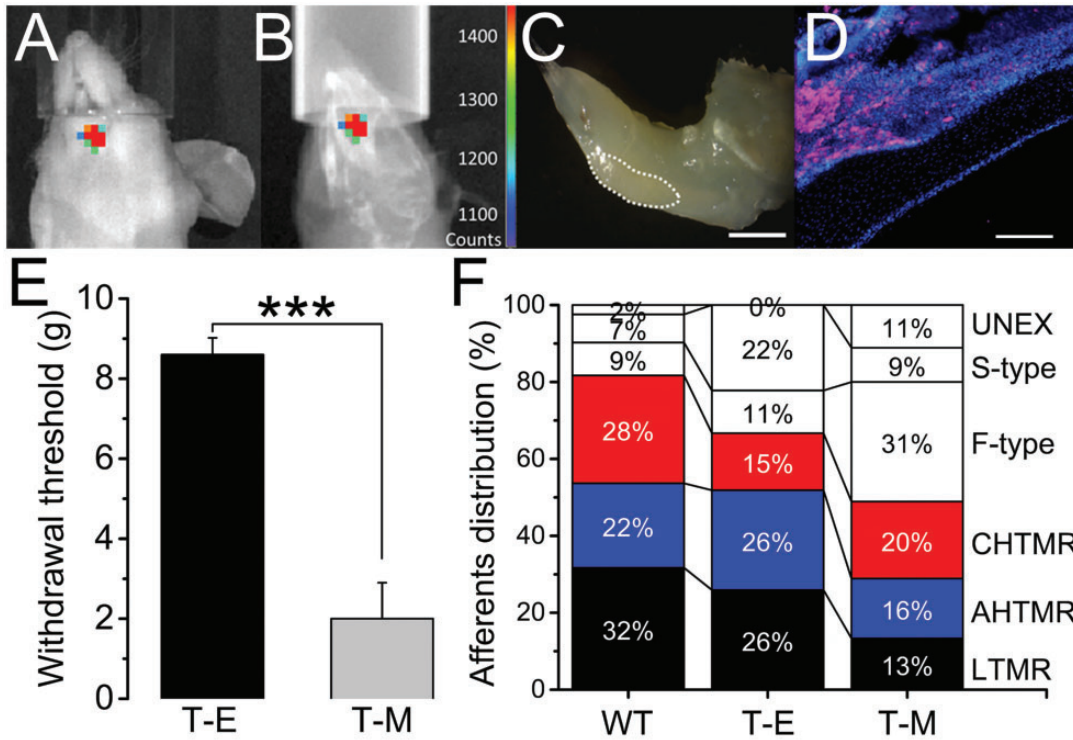


Figure 2. Overlapped image of (a) bioluminescence and (b) X-ray of the mandible of a *Foxn1* mouse 3 weeks after intracardiac injection of MDA-MB-231^{LUC+} cancer cells (color-coded counts, sidebar). (c) Location in the left mandible in this animal of the tumor-induced bone lesion (dotted white line). (d) Stained section of the lesion for luciferase (pink) and DAPI (blue). (e) Effects of tumor implantation on the reflexive head withdrawal (T-E vs. T-M) (***) ($p < 0.001$). (f) Distribution (in %) of TG recorded afferents per animal per treatment (WT vs. T-E vs. T-M). Scale bar: 1 mm, 100 μ m.

Table 1. Conduction velocity and somatic active electrical properties (SAP) in TG tactile (LTMR) and nociceptive (AHTMR and CHTMR) mechanosensory afferents recorded from C57BL6/J (WT) and *Foxn1* (T-E and T-M) mice.

		Trigeminal sensory neurons							
		Somatic active properties (SAP)							
				Spike				AHP	
Type	N	CV m/sec	Amplitude, mV	D50, ms	MDR, dV/s	MRR, dV/s	Amplitude, mV	AHP50, ms	
WT	LTMR	26	10 \pm 1.3	37 \pm 3 ^{###}	0.7 \pm 0.03 ^{###}	123 \pm 12 [#]	-118 \pm 27 [#]	5 \pm 0.9	3 \pm 0.6
	AHTMR	18	4 \pm 0.6	54 \pm 3	1.6 \pm 0.1	81 \pm 12	-58 \pm 11	8 \pm 1 [‡]	8 \pm 1.4 ^{##}
	CHTMR	23	0.4 \pm 0.1	56 \pm 2	2.5 \pm 0.2	69 \pm 5	-30 \pm 4	15 \pm 1.9 ^{##}	11 \pm 1.6 ^{##}
T-E	LTMR	7	19 \pm 7	44 \pm 8 [#]	0.5 \pm 0.2 ^{###}	127 \pm 7	-96 \pm 27	9 \pm 3.5	9 \pm 3.4 [†]
	AHTMR	7	14 \pm 4	70 \pm 2	2 \pm 0.4	113 \pm 23	-59 \pm 13	15 \pm 3.5	15 \pm 3.6
	CHTMR	4	0.5 \pm 0.1	68 \pm 6	2.2 \pm 0.2	132 \pm 2	-47 \pm 4	21 \pm 2.3 [‡]	10 \pm 2.9
T-M	LTMR	6	14 \pm 3	48 \pm 6 [#]	0.9 \pm 0.1 [#]	95 \pm 18 [†]	-60 \pm 7 ^{††}	10 \pm 3.7	4 \pm 1.1
	AHTMR	7	10 \pm 3	65 \pm 3	1.8 \pm 0.2	114 \pm 18	-60 \pm 7	16 \pm 3.4	10 \pm 2.9
	CHTMR	9	0.6 \pm 0.2	64 \pm 3	2.5 \pm 0.4	95 \pm 16	-41 \pm 7	18 \pm 2.2	12 \pm 2.9

Data are medians presented \pm standard error. Symbols (Bonferroni correction test applied):

[#]Significant difference between LTMR and HTMR per group (#: $p < 0.05$; ###: $p < 0.01$).

[†]Significant difference between WT and T-M/T-E LTMRs (†: $p < 0.05$; ††: $p < 0.01$).

[‡]Significant difference between HTMR and LTMR per group (‡: $p < 0.05$; ‡‡: $p < 0.01$).

As previously described,²⁶ LTMR afferents have significantly smaller AHP amplitude and shorter AHP duration than HTMR afferents, although this was not the case in **T-M** animals, due to a significant ($p < 0.05$) increase in the LTMR AHP amplitude and increased variability in the AHP duration (Table 1).

c. *Mechanical sensibility (MT^l)*: As shown in Figure 3 (a), mechanical thresholds of all three subtypes of mechanosensory afferents were significantly different in WT animals (LTMR vs AHTMR: $p < 0.001$ and AHTMR vs CHTMR: $p < 0.01$), regardless of the innervation area. Mechanical threshold was also significantly ($p < 0.01$) lower in LTMR than HTMR

afferents in **T-E** animals, although AHTMR and CHTMR afferents did not differ significantly, perhaps due to the small sample size (Figure 3(b)).

Of note, the difference between the MT of AHTMR and CHTMR in WT animals was determined by the presence of 4 AHTMR V1/2 afferents with exquisite sensibility (median: 1.1 mN [range: 0.39 to 1.57 mN]) innervating the eyelids and lacrimal areas.²³ Among groups (**WT** vs. **T-E**), no significant difference was observed between AHTMR and CHTMR afferents. However, LTMR afferents recorded from **T-E** animals were observed to be significantly ($p < 0.05$) less sensitive than similar afferents recorded from **WT** animals.

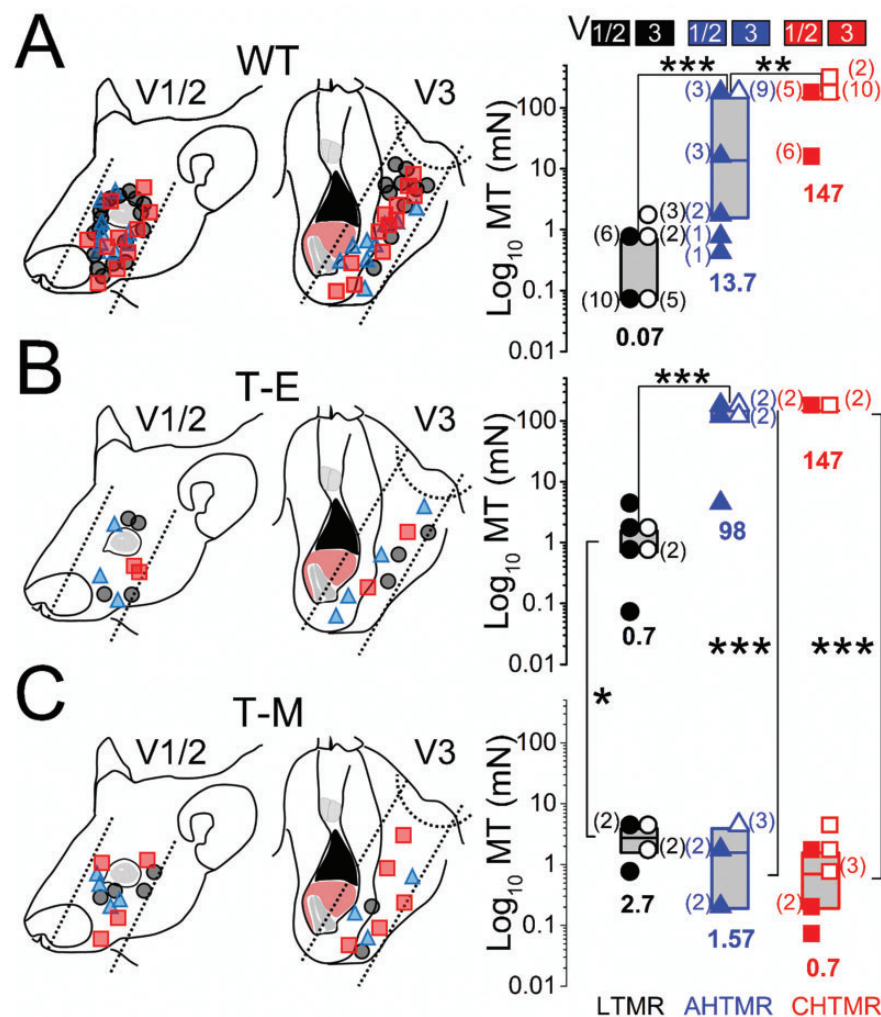


Figure 3. Schematic diagram of the receptive field locations of recorded afferents and their presumed trigeminal nerve divisions in (a) Wild type (WT), (b) MDA-MB-231^{LUC+} tumor elsewhere from head and neck (T-E), and (c) MDA-MB-231^{LUC+} tumor in left mandible (T-M) mice. Data are presented with the location and subtype (right) (●: LTMR; ▲: AHTMR; ■: CHTMR) of recorded afferents. Mechanical threshold (MT) of subtypes of afferents according to trigeminal division: V1/2 (solid symbol) and V3 (open symbol). Individual data points and medians (horizontal bars, values at the bottom) with boxes representing the 25 and 75 percentiles. The number of afferents per MT is presented beside in parentheses. *= $p < 0.05$, **= $p < 0.01$, ***= $p < 0.001$.

In contrast to afferents in **T-E** animals, afferent classes could not be distinguished at all by the mechanical threshold in **T-M** afferents (Figure 3(c)). Furthermore, LTMRs (median: 2.7 [range 0.7 to 3.9 mN]) were significantly less sensitive than similar afferents recorded from **T-E** animals ($p < 0.05$). Similarly, HTMRs in **T-M** animals were significantly more sensitive than similar afferents recorded from **T-E** ($p < 0.001$) animals (AHTMR median: 1.57 mN [range 0.19 to 3.9 mN] and CHTMR median: 0.7 mN [range 0.07 to 3.9 mN]).

Post-discharge hyperpolarization (PDH): As previously described,⁵¹ AHTMRs, reacted to activation with a long-lasting (hundreds of milliseconds) hyperpolarization of their cellular membrane potential after the initial discharge to mechanical stimulation. AHTMR afferents in both **WT** (12/18, 67%) and **T-E** (7/7, 100%) animals showed a similar magnitude of membrane hyperpolarization after activation (WT: 10.1 ± 1.9 mV and **T-E**: 8.4 ± 2.2 mV). In contrast, none of the AHTMR afferents recorded from **T-M** animals exhibited PDH after activation (0/7, 0%).

Immunohistochemistry

Contralateral. SP immunoreactivity was present in 12 of the 60 cells (20%), widely distributed among small to medium cells (median: 24 μ m [range: 14 to 30 μ m]). All SP immunoreactive cells co-expressed CGRP but at a significantly ($p < 0.01$) lower immunoreactivity (Figure 4(a) and (c)).

CGRP immunoreactivity was observed in 40 of the 60 cells (67%), with only 28 cells (47%) co-reactive to SP. These cells were broadly distributed among small to large diameters (median: 25 μ m [range: 17 to 38 μ m]) (Figure 4(a) and (c)).

Double negatives (-/-): immunoreactivity to SP or CGRP was absent in 20/60 cells (33%). The distribution of these cells' diameter overlapped both SP and CGRP populations (median: 23 μ m [range: 13 to 36 μ m]) (Figure 4(a)).

Ipsilateral

SP immunoreactivity was present in 11 of the 73 cells (15%). Nine of these SP immunoreactive cells were also reactive to CGRP. In contrast to the contralateral side, immunoreactivity of cells co-expressing SP and CGRP was similar in density for the two peptides (Figure 4(b) and (c)).

CGRP immunoreactivity was present in 39 of the 73 cells (53%), with 30 of these reactive to CGRP. As with the SP, these cells' size distribution also extended to larger diameter cells (median: 25 μ m [range: 11 to 54 μ m]), but without significant change in their immunoreactivity (see above) (Figure 4(b) and (c)).

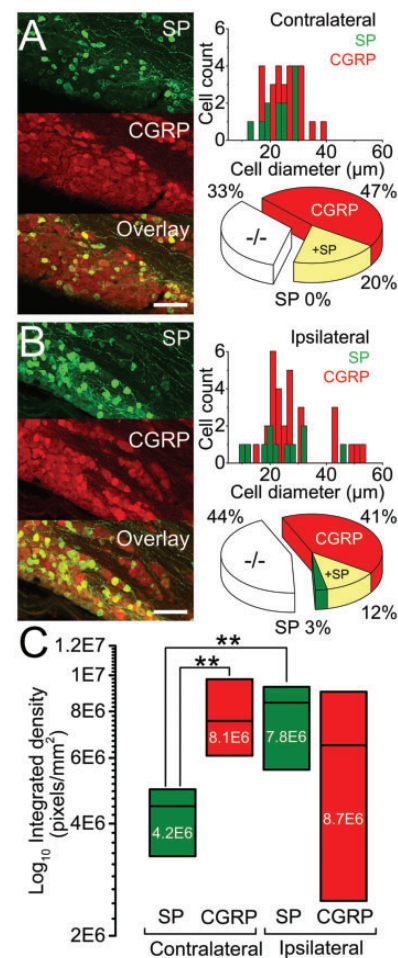


Figure 4. Representative SP (green), CGRP (red), and their overlay immunoreactivity in sections of trigeminal ganglia (TG) visualized by confocal microscopy. Data ((a) contra and (b) ipsilateral) are presented with the cell count per cell diameter (bin 2, μ m, left column) and proportional distribution (pie charts, middle column). (c) Immunoreactivity integrated density (pixels/mm², right column), three weeks after MDA-MB-231^{LUC+} tumor left mandible implantation. ** = $p < 0.01$ between SP and CGRP. Scale bar: 100 μ m.

Double negatives (-/-): immunoreactive to SP or CGRP was absent in 32/73 cells (44%). Again, and as observed in the contralateral side, the distribution of these cells' diameter overlapped both SP and CGRP populations (median: 21 μ m [range: 8 to 58 μ m]) (Figure 4(b)).

Cellular response and sensitization by CSn application

Response: Injection of control media diluted in artificial CSF experiments did not alter cell basal properties or response to stimulation in any of the 36 sensory afferents studied. In contrast, cells exposed to CSn robustly reacted in a modality-specific manner (Figure 5(a)). None of the LTMRs spontaneously discharged after

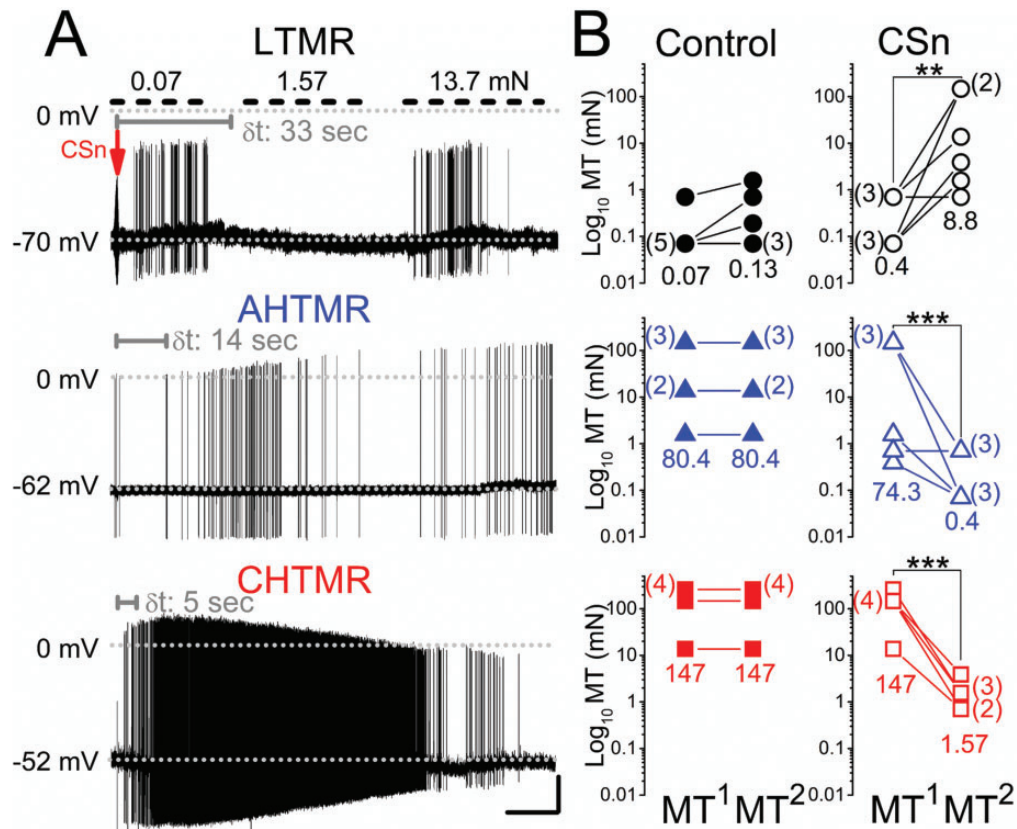


Figure 5. (a) Response of a low, A-high, and C-high threshold mechanoreceptor (LTMR, AHTMR, CHTMR respectively) afferent after subcutaneous injection at the arrow of the supernatant of MDA-MB-231^{LUC+} cancer cell cultures (CSn) into their receptor field. Mechanical stimulation is only applied to LTMRs (upper short-dashed bars). Note the delay in the afferent's response (δt in sec, gray) to loss of response to stimulation in the LTMR and onset of spontaneous activity in the HTMRs and the differential modulation on the AP amplitude during and with ongoing discharge in the HTMRs. (b) Effects of CSn injection on mechanical threshold (MT) (●: LTMR; ▲: AHTMR; ■: CHTMR). Numbers are medians of thresholds before (MT¹) and after (MT²), control or CSn injection. The number of afferents per MT is presented aside in parentheses. **= $p < 0.01$, ***= $p < 0.001$. Scale bars: 15 sec, 20 mV

CSn injection, although 5 of 6 cells showed sensitization, discussed below, with a delay from the injection (δt) of 31.2 ± 1.8 sec. AHTMRs (5 of 6) and all CHTMRs responded significantly faster ($p < 0.001$) with spontaneous discharge (AHTMR δt : 13.8 ± 2 sec and CHTMR δt : 4.3 ± 0.7 sec). Spontaneous discharge in AHTMRs lasted 29 ± 18 sec (# of APs; median 16 APs/response [range: 14 to 57 APs/response]; IFmax: median 26 [range: 3.6 to 75 Hz]). In 3 of the 6 cells this response led to spontaneous activity for > 2 min. The CHTMR response lasted 50 ± 14 sec (# of APs; median 40 APs/response [range 12 to 750 APs/response]; IFmax: median 23 Hz [range: 10 to 43 Hz]). In 4 of the 6 cells, this response led to spontaneous activity for > 2 min.

Somatic active electrical properties: The cellular response to CSn led to alterations in AP shape in HTMRs during the 2 min observation period. **AHTMRs:** Spike duration (D50) was reduced from 1.9 ± 0.1 ms to 0.7 ± 0.1 ms at the end of the 2 min observation ($p < 0.001$), although spike amplitude did not

change (55 ± 3.3 mV before to 66 ± 5.6 mV at the end of the 2 min observation). AHP duration (AHP50) was also significantly ($p < 0.01$) reduced 11 ± 2 mV to 5 ± 0.7 mV from CSn injection, whereas AHP amplitude was not changed (initial: 9.2 ± 0.7 mV to end: 11 ± 2.3 mV). **CHTMRs:** Spike duration was increased by CSn injection from 2.5 ± 0.2 ms to 3.9 ± 0.5 ms, accompanied by a reduction in their spike amplitude from 65 ± 1.3 mV to 57 ± 1.8 mV ($p < 0.01$). In contrast to AHTMRs, CSn injection did not affect AHP in CHTMRs, either in amplitude (14 ± 8 mV to 17 ± 3.7 mV) or in duration (9 ± 3.2 ms to 13 ± 1.2 ms).

Sensitization: As shown in Figure 5(b), injection of aCSF control did not modify the MT of the studied sensory afferents. However, CSn injection modulated afferent mechanical sensibility in a modality-specific manner. LTMRs desensitized to mechanical stimulation steadily over the 2 min observation period. Two minutes after CSn injection, the MT of these afferents significantly ($p < 0.01$) increased 22-fold and in some cases (2/6)

become mechanically insensitive soon after the MT² was measured. In contrast, HTMR afferents were significantly ($p < 0.001$) sensitized, with MT decreased (AHTMRs: 186-fold and CHTMRs: 94-fold) after CSn injection.

Discussion

Cancer cells are known to produce metabolic mediators capable of activating sensory neurons. This study uncovers profound effects on the peripheral sensibility consistent with signs and symptoms reported by human patients underlining the importance of the peripheral system in response to tumor growth. The principal observations of our studies are that the xenograft cancer model created by the use of MDA-MB-231^{LUC+} successfully recreate several aspects of sensorial neuropathy and symptomatology as observed in human patients,⁵⁴ that this sensorial neuropathy is not restricted to the cancer microenvironment but widespread across the TG dermatome,⁴² and the increased expression of neuropeptides related to the neurogenic ganglionic response.³⁹ We have also observed that metabolic products obtained from these cancer cells (CSn) induce an acute sensorial response in the absence of tissue damage.²²

Together, our observations indicate that this cancer cell line activity can modulate TG peripheral sensory excitability and trigger an enhanced non-local neuronal response. Our results also suggest that this interaction is not unidirectional, and the sensorial response may also be modulatory effects on the carcinogenesis. These results allow us to speculate on the consequences of this bidirectional interaction in the context of neurogenic control of tumor growth.

Technical considerations

This study is largely restricted to the neuronal mechanical sensibility. Other parameters such as cellular responsiveness and thermal sensibility are not studied. Although useful, mechano-sensibility alone does not provide a complete measure of the enhanced activity of the sensory system or the magnitude of cancer-induced modulation of the peripheral system.

Human breast cancer xenografts model for the study of JMCB related pain

The use of MDA-MB-231^{LUC+} is fully justified by its ability to naturally invade the animals' mandible. This cancer line it has been reported to be 100% efficient to spread to the female animals' mandible.³⁵ As expected, the efficiency of this cell line in male animals was far less than reported, reaching only 35%. The causes for this

differential efficacy are intuitive due to the sex-specific origin (female) of this cell line. However, it is possible that the use of a different animal breed on the generation of the nude mice (Balb/c vs. C57BL6/J) may have some impact on the differential cellular implantation ratio. Unfortunately, there's not enough information on this animal's physiology to speculate further on the importance of this difference to explain the discrepancy.

On the other hand, sex differences may be crucial to the process. As recently reviewed by Shin et al., sex-bias disparities have been shown to be one of the critical factors underlining the incidence and mortality of cancer.⁵⁵ From the cancer cells perspective, there is abundant evidence that male and female cancer cell lines differentially expressed genes and proteins that may have an influence on their sex-specific carcinogenic capabilities.^{56–58} However, from the peripheral somatosensory physiology standpoint, there is no evidence of sex-bias in the response of TG sensory neurons to injury. Further studies using B6.Cg Foxn1nu/J females with a breed of both origins (Balb/c vs. C57BL6/J) are needed to validate this assumption and to perfect this model.

Do sensory symptoms precede gross tumor presence and local tissue damage?

Cancer pain pathophysiology largely depends on the cancer heterogeneity, type, and anatomic locations of the tumors. Cancer-associated facial pain introduces an even greater complexity since some reports indicated that it could arise from regional or distant tumor effects or even a consequence of cancer therapy.⁵⁹

In this context, although rare, metastases to the jaw are reported to induce cancer-associated sensory disruptions. These reports also indicate the presence of both local and widespread disturbances on the trigeminal domain, not always consistent with the magnitude of the damage generated by the tumor^{7–10} or even its location within the affected region.⁶⁰ Symptoms and clinical signs of this disease are also variable and can be concurrent, ranging from mild local hypoesthesia¹⁰ to widespread orofacial pain and, in some extreme cases, trigeminal neuralgia.⁵⁹

Unfortunately, the available literature on the topic is mostly based on case reports rather than systematic studies due to a lack of appropriate animal models. Together, these reports indicate that the interaction between the disease and the trigeminal sensory system is complex and non-related to the magnitude of the tissue damage at the region of the tumor implantation (regional or distal). The anatomical and methodological limitations imposed by the unique location and specialized tissues innervated by the TG are also contributing factors to the absence of systematic animal studies on the cancer-neurons interaction in the facial region.

The current study has overcome both limitations, and our results largely argue in favor of using naturally implanted MDA-MB-231^{LUC+} based mandibular tumor (JMCB) as an appropriate tool to recreate some key features of the patient's symptomatology. Our observations are consistent with the simultaneous development of a local and regional neuropathy that involves both nociceptive and non-nociceptive mechanosensory afferents. These observations also concur with the notion that some aspect of the sensory disruption described in cancer-induced facial pain may not be causally related to the tumor growth or the damaged tissues (see below).

Balance of tactile/nociceptor input to the experience of pain and role of cancer metastasis to bone

Despite the above-mentioned clinical reports indicating regional and distal effects of cancer implantation on the TG system, many preclinical studies focus on the local cancer-microenvironment. Such studies mainly show that cancer-induced pain is likely to be a result of the sensitization or activation of primary nociceptive afferents by mediators liberated by cancer and associated cells⁶¹⁻⁶³ exacerbated by the mechanical function involving mechanical allodynia and hyperalgesia.³

On the TG system, similar nociceptive sensitization has been observed in several injury nerve injury models. However, since such models fail to evaluate non-local effects of injury in one branch of the TG over the others,^{17,64,65} our expectations prior to this study were modest, mostly anticipating local sensorial changes on the affected branch (V3). Unexpectedly, we observed that JMCB induced a widespread disruption in the TG sensory neurons' mechanical sensibility, extending to the whole TG ipsilateral dermatome.

As described by our results, JMCB induces a profound change in the distribution and sensibility of different subtypes of mechanosensory afferents. While inducing nociceptive sensitization, it also increases the mechanical threshold of tactile afferents (desensitization), affecting the whole of the TG dermatome. These observations are consistent with reports of widespread sensitization effects (trigeminal neuralgia) in human (head and neck) cancer patients^{66,67} and widespread ganglionic propagation of inflammatory signaling after localized pronociceptive stimulation in the trigeminal system of rats.^{64,68}

Although this is the first report of such changes on the peripheral sensibility in the TG due to a local injury, similar sensorial effects have been described in other dermatomes. This abrupt change in the distribution, sensibility and electrical properties of both tactile and nociceptive afferents has been observed to affect both damage and undamaged afferents after dissimilar types

of injury (acute and chronic)^{39,42,69,70} and pronociceptive stimulation.⁵⁴ In the same way, the absence of PDH on the T-M group is indicative of an hyperexcitable state, that as described,⁵¹ contribute to increase the cellular responsiveness after sensitization.

The consistency of these changes in the normal activation patterns of the peripheral system is puzzling. As argued in Boada et al., these changes indicate the peripheral sensory system's pivotal role in developing pain neuropathies of various origins.⁷¹ Our results extend this statement further into the effects of JMCB on the TG sensory system, highlighting the role of fast conducting afferents (nociceptive [AHTMRs] and non-nociceptive [LTMR]) as important contributors to the patients reported symptomatology.

Early role of cancer secreted products on the sensory disruption

As argued by Scheff et al. the use of cancer supernatant (CSn) (by injection [*in vivo*] or infusion [*in vitro*] may provide a useful tool for the analysis of secreted mediators' nociceptive effect without the impact of tumor burden and systemic illness that accompanies carcinogenesis.⁷² Although sensical, the literature on this approach is scarce (only two manuscripts have been identified), and the results are variable. The description of the putative pronociceptive effects of the CSn relies almost entirely upon assessing reflexive⁷³ and non-reflexive⁷² animal behaviors, performed consecutively from hours⁷³ to days⁷² after several CSn injections on the tissue target. Furthermore, the above-mentioned manuscripts use different cancer cell subtypes (human pancreatic cell line [SW1990]⁷³ and human tongue carcinoma cell lines [HSC-3 and SCC9]⁷² as the source of their CSn.

These differences in methodology (among many others), together with the likelihood of different compositions of the secretions of these cell lines, greatly limited the interpretability of the reported effects of the CSn and its use for the study of the cancer cells-sensory neurons interaction. Nevertheless, an important point addressed in both manuscripts seems to be consistent. In both cases, CSn does induce local sensitization and the modulation of the excitability of the sensory neurons. This is important for two reasons: a) It indicates the pivotal role of the secreted nociceptive mediators as the more likely primary etiology of cancer pain⁷² b) it implicates the normal sensory response (and neuronal secretions products [SP and CGRP])^{38,73} to the CSn as an initial crucial link for the cancer cells-sensory neurons crosstalk.

Our results using CSn (obtained from human breast cancer cell line MDA-MB-231^{LUC+}) concur with the electrophysiological aspects of both studies and extend these manuscript observations to the initial sensory consequences of the CSn injection. Although the observed

effects' magnitude cannot be directly translated to different cell lines, the speed of its development signals a direct sensorial effect. Furthermore, its selectivity modulating the sensibility of both nociceptive and non-nociceptive mechanosensory afferents clearly indicates its effectiveness in modulating the overall peripheral mechanical sensibility as a whole.

Robinson et al. ponders on the need for spontaneous and mechanically induced neuronal discharge from the injury site to play a crucial role in the widespread and chronification of pain.⁶⁴ Although this notion may justify a centrally mediated sensitization, it fails to explain the observed effects on uninjured afferents innervating distal portions of the TG dermatome. Although possible, the likelihood of axonal reflexes or nerve crosstalk as responsible for the observed extensive sensitization is extremely low due to the unique anatomy of the TG. Other aspects relevant to the cancer-sensory neuron interaction (as transganglionic activation [microglia]⁷⁴ and immune response⁷⁵) could be more appropriate to explain this observation on the non-local peripheral effects of the early tumor implantation and warrant further studies.

Role of neuropeptides on the pathophysiology of cancer/sensory neurons interaction

It has been shown that injury or disease induces the orthodromic activation of nociceptive sensory neurons. This activation often induces the antidromic release of their bioactive contents into surrounding tissues (neurogenic inflammation).⁷⁶ This bioactive content includes several neuropeptides necessary for the normal nociceptive activation⁵² but also with well-recognized pro-tumorigenic functions (SP and CGRP) via cancer cells expression of these peptides receptors.³⁸

Concurrently, some aggressive cancer cell lines (SW1990⁷³ and MDA-MB-231³⁸) release several molecules or their precursors (trypsin⁷³ and bradykinin³⁸) that can trigger the neurogenic inflammatory response, the release of the neuronal bioactive content,⁷³ and the increase of the cancer cell expression of their receptors.³⁸

These observations indicate the existence of a functional loop of cross-activation between cancer cells and primary sensory neurons, likely mediated by a molecular exchange of bioactive contents (pro-nociceptive and pro-tumorigenic) with paracrine and autocrine functions.³⁸

In this context and as expected, the current study shows that JMCB does induce an increased expression and production (*de novo* synthesis) of neuropeptides on the TG. Although consistent with the proposed autocrine functions of these neuropeptides⁵² and the observed widespread hyperexcitability, our interpretation of these overexpression consequences is limited by several factors. While the expression and *de novo*

synthesis can be correlated with the cellular size, in our study, we did not attempt to identify the modality of the afferents overexpressing these peptides nor their direct innervation of the tumor. Furthermore, we recognize that this correlation does not reflect causality. Therefore, further functional and pharmacological studies should be designed to target the proposed cancer-sensory neurons loop at its apparent weaker link: neuropeptides receptors (NK1R in particular³⁸) after and before MDA-MB-231^{LUC+} tumor implantation.

Conclusions

The current study has unmasked the profound peripheral sensory effects of tumor growth in the TG system. We have demonstrated that with some restrictions' in the probability of implantation, MDA-MB-231^{LUC+} can be a useful tool for the study of cancer-induced facial pain and gender differences in the TG system.

Widespread disruption affecting different cellular modalities is consistent with the development of peripheral neuropathy. Although some aspects of these hallmarks can be reproduced by the application of CSn, the correlations between the direct activation of the afferents innervating the tumor and the overall sensitization process remain unclear.

Although we have established the sensorial effects of tumor implantation, the concurrent consequences of the overexpression of neuronal neuropeptides (SP and CGRP) on tumor growth are less clear. Specific studies to evaluate this interaction need to be performed in this *in vivo* model (or similar) combined with selective receptor antagonists and tachykinin knock-out (B6.Cg-Tac1tm1Bbm/J termed Tac1 KO)⁵² animals so the relevance of this interaction can be established.

Acknowledgments

In loving memory of Rafaela Endara-Maldonado and Juan Bernardo Boada-Bustos.

Declaration of Conflicting Interests

The author(s) declared no potential conflicts of interest with respect to the research, authorship, and/or publication of this article.

Funding

The author(s) disclosed receipt of the following financial support for the research, authorship, and/or publication of this article: This work was supported by grant P01 NS113852 (JCE and MDB) from the National Institutes of Health.

ORCID iD

M Danilo Boada  <https://orcid.org/0000-0002-8973-3010>

References

1. Schmidt BL, Hamamoto DT, Simone DA, Wilcox GL. Mechanism of cancer pain. *Mol Interv* 2010; 10: 164–178.
2. Reyes-Gibby CC, Anderson KO, Merriman KW, Todd KH, Shete SS, Hanna EY. Survival patterns in squamous cell carcinoma of the head and neck: pain as an independent prognostic factor for survival. *J Pain* 2014; 15:1015–1022.
3. Lam DK, Schmidt BL. Orofacial pain onset predicts transition to head and neck cancer. *Pain* 2011; 152: 1206–1209.
4. Mantyh PW. The neurobiology of skeletal pain. *Eur J Neurosci* 2014; 39: 508–519.
5. Oliveira KG, von Zeidler SV, Lamas AZ, Podestá JR, Sena A, Souza ED, Lenzi J, Lemos EM, Gouvea SA, Bissoli NS. Relationship of inflammatory markers and pain in patients with head and neck cancer prior to anticancer therapy. *Braz J Med Biol Res* 2014; 47: 600–604.
6. Sato J, Fujiwara M, Kawakami T, Sumiishi A, Sakata S, Sakamoto A, Kurata A. Fascin expression in dendritic cells and tumor epithelium in thymoma and thymic carcinoma. *Oncol Lett* 2011; 2: 1025–1032.
7. Kumar G, Manjunatha B. Metastatic tumors to the jaws and oral cavity. *J Oral Maxillofac Pathol* 2013; 17: 71–75.
8. Anderson RS, Peeples WJ. Mandibular osseous metastasis from esophageal carcinoma: a case report and review of the literature. *J Oral Maxillofac Surg* 1990; 48: 188–192.
9. Burt RK, Sharfman WH, Karp BI, Wilson WH. Mental neuropathy (numb chin syndrome). A harbinger of tumor progression or relapse. *Cancer* 1992; 70: 877–881.
10. Irani S. Metastasis to the Jawbones: a review of 453 cases. *J Int Soc Prev Community Dent* 2017; 7: 71–81.
11. Bullitt E, Tew JM, Boyd J. Intracranial tumors in patients with facial pain. *J Neurosurg* 1986; 64: 865–871.
12. Cheng TM, Cascino TL, Onofrio BM. Comprehensive study of diagnosis and treatment of trigeminal neuralgia secondary to tumors. *Neurology* 1993; 43: 2298–2302.
13. Reddy GD, Wagner K, Phan J, DeMonte F, Raza SM. Management of skull base tumor-associated facial pain. *Neurosurg Clin N Am* 2016; 27: 337–344.
14. Schmidt RF, Yick F, Boghani Z, Eloy JA, Liu JK. Malignant peripheral nerve sheath tumors of the trigeminal nerve: a systematic review of 36 cases. *Neurosurg Focus* 2013; 34: E5.
15. Moran LB, Graeber MB. The facial nerve axotomy model. *Brain Res Brain Res Rev* 2004; 44: 154–178.
16. Pozza DH, Castro-Lopes JM, Neto FL, Avelino A. Spared nerve injury model to study orofacial pain. *Indian J Med Res* 2016; 143: 297–302.
17. Vos BP, Strassman AM, Maciewicz RJ. Behavioral evidence of trigeminal neuropathic pain following chronic constriction injury to the rat's infraorbital nerve. *J Neurosci* 1994; 14: 2708–2723.
18. Chodroff L, Bendele M, Valenzuela V, Henry M, Ruparel S. EXPRESS: BDNF signaling contributes to oral cancer pain in a preclinical orthotopic rodent model. *Mol Pain* 2016; 12: 1744806916666841.
19. Nagamine K, Ozaki N, Shinoda M, Asai H, Nishiguchi H, Mitsudo K, Tohnai I, Ueda M, Sugiura Y. Mechanical allodynia and thermal hyperalgesia induced by experimental squamous cell carcinoma of the lower gingiva in rats. *J Pain* 2006; 7: 659–670.
20. Ono K, Harano N, Inenaga K, Nakanishi O. A rat pain model of facial cancer. *Methods Mol Biol* 2012; 851: 149–157.
21. Fried K, Hansson PT. Animal models of trigeminal neuralgia: a commentary. *Mol Pain* 2020; 16: 1744806920980538.
22. Boada MD, Houle TT, Eisenach JC, Ririe DG. Differing neurophysiologic mechanosensory input from glabrous and hairy skin in juvenile rats. *J Neurophysiol* 2010; 104: 3568–3575.
23. Boada MD. Relationship between electrophysiological signature and defined sensory modality of trigeminal ganglion neurons in vivo. *J Neurophysiol* 2013; 109: 749–757.
24. Sabino MA, Luger NM, Mach DB, Rogers SD, Schwei MJ, Mantyh PW. Different tumors in bone each give rise to a distinct pattern of skeletal destruction, bone cancer-related pain behaviors and neurochemical changes in the central nervous system. *Int J Cancer* 2003; 104: 550–558.
25. Schmidt BL. The neurobiology of cancer pain. *Neuroscientist* 2014; 20: 546–562.
26. Kristiansen KA, Edvinsson L. Neurogenic inflammation: a study of rat trigeminal ganglion. *J Headache Pain* 2010; 11: 485–495.
27. Sio SW, Puthia MK, Lu J, Moochhala S, Bhatia M. The neuropeptide substance P is a critical mediator of burn-induced acute lung injury. *J Immunol* 2008; 180: 8333–8341.
28. Lam DK, Dang D, Zhang J, Dolan JC, Schmidt BL. Novel animal models of acute and chronic cancer pain: a pivotal role for PAR2. *J Neurosci* 2012; 32: 14178–14183.
29. Holzer P. Local effector functions of capsaicin-sensitive sensory nerve endings: involvement of tachykinins, calcitonin gene-related peptide and other neuropeptides. *Neuroscience* 1988; 24: 739–768.
30. Richardson JD, Vasko MR. Cellular mechanisms of neurogenic inflammation. *J Pharmacol Exp Ther* 2002; 302: 839–845.
31. Coveñas R, Muñoz M. Cancer progression and substance P. *Histol Histopathol* 2014; 29: 881–890.
32. Muñoz M, Coveñas R. Involvement of substance P and the NK-1 receptor in cancer progression. *Peptides* 2013; 48: 1–9.
33. Muñoz M, Coveñas R. Involvement of substance P and the NK-1 receptor in human pathology. *Amino Acids* 2014; 46: 1727–1750.
34. Rosso M, Muñoz M, Berger M. The role of neurokinin-1 receptor in the microenvironment of inflammation and cancer. *Sci World J* 2012; 2012: 381434.
35. Hwang YS, Han SS, Kim KR, Ye-Jin L, Sun-Kyung L, Kwang-Kyun P, Won-Yoon C. Validating of the pre-clinical mouse model for metastatic breast cancer to the mandible. *J Appl Oral Sci* 2015; 23: 3–8.
36. Roux SL, Borbely G, Słoniecka M, Backman LJ, Danielson P. Transforming growth factor beta 1 modulates the functional expression of the neurokinin-1 receptor in human keratocytes. *Curr Eye Res* 2016; 41: 1035–1043.

37. Zhang L, Hoff AO, Wimalawansa SJ, Cote GJ, Gagel RF, Westlund KN. Arthritic calcitonin/alpha calcitonin gene-related peptide knockout mice have reduced nociceptive hypersensitivity. *Pain* 2001; 89: 265–273.
38. Gutierrez S, Boada MD. Neuropeptide-induced modulation of carcinogenesis in a metastatic breast cancer cell line (MDA-MB-231LUC+). *Cancer Cell Int* 2018; 18: 216.
39. Boada MD, Gutierrez S, Giffear K, Eisenach JC, Ririe DG. Skin incision-induced receptive field responses of mechanosensitive peripheral neurons are developmentally regulated in the rat. *J Neurophysiol* 2012; 108: 1122–1129.
40. Minn AJ, Kang Y, Serganova I, Gupta GP, Giri DD, Doubrovin M, Ponomarev V, Gerald WL, Blasberg R, Massagué J. Distinct organ-specific metastatic potential of individual breast cancer cells and primary tumors. *J Clin Invest* 2005; 115: 44–55.
41. Ye Y, Dang D, Viet CT, Dolan JC, Schmidt BL. Analgesia targeting IB4-positive neurons in cancer-induced mechanical hypersensitivity. *J Pain* 2012; 13: 524–531.
42. Boada MD, Gutierrez S, Aschenbrenner CA, Houle TT, Hayashida K, Ririe DG, Eisenach JC. Nerve injury induces a new profile of tactile and mechanical nociceptor input from undamaged peripheral afferents. *J Neurophysiol* 2015; 113: 100–109.
43. Wellnitz SA, Lesniak DR, Gerling GJ, Lumpkin EA. The regularity of sustained firing reveals two populations of slowly adapting touch receptors in mouse hairy skin. *J Neurophysiol* 2010; 103: 3378–3388.
44. Boada MD, Woodbury CJ. Myelinated skin sensory neurons project extensively throughout adult mouse substantia gelatinosa. *J Neurosci* 2008; 28: 2006–2014.
45. Boada MD, Woodbury CJ. Physiological properties of mouse skin sensory neurons recorded intracellularly in vivo: temperature effects on somal membrane properties. *J Neurophysiol* 2007; 98: 668–680.
46. Garell PC, McGillis SL, Greenspan JD. Mechanical response properties of nociceptors innervating feline hairy skin. *J Neurophysiol* 1996; 75: 1177–1189.
47. Slugg RM, Meyer RA, Campbell JN. Response of cutaneous A- and C-fiber nociceptors in the monkey to controlled-force stimuli. *J Neurophysiol* 2000; 83: 2179–2191.
48. Gallego R, Eyzaguirre C. Membrane and action potential characteristics of A and C nodose ganglion cells studied in whole ganglia and in tissue slices. *J Neurophysiol* 1978; 41: 1217–1232.
49. Yoshida S, Matsuda Y. Studies on sensory neurons of the mouse with intracellular-recording and horseradish peroxidase-injection techniques. *J Neurophysiol* 1979; 42: 1134–1145.
50. Cabanes C, López de Armentia M, Viana F, Belmonte C. Postnatal changes in membrane properties of mice trigeminal ganglion neurons. *J Neurophysiol* 2002; 87: 2398–2407.
51. Boada MD, Ririe DG, Eisenach JC. Post-discharge hyperpolarization is an endogenous modulatory factor limiting input from fast-conducting nociceptors (AHTMRs). *Mol Pain* 2017; 13: 1744806917726255.
52. Gutierrez S, Alvarado-Vázquez PA, Eisenach JC, Romero-Sandoval EA, Boada MD. Tachykinins modulate nociceptive responsiveness and sensitization: In vivo electrical characterization of primary sensory neurons in tachykinin knockout (Tac1 KO) mice. *Mol Pain* 2019; 15: 1744806919845750.
53. Jimenez-Andrade JM, Bloom AP, Stake JI, Mantyh WG, Taylor RN, Freeman KT, Ghilardi JR, Kuskowski MA, Mantyh PW. Pathological sprouting of adult nociceptors in chronic prostate cancer-induced bone pain. *J Neurosci* 2010; 30: 14649–14656.
54. Boada MD, Eisenach JC, Ririe DG. Mechanical sensibility of nociceptive and non-nociceptive fast-conducting afferents is modulated by skin temperature. *J Neurophysiol* 2016; 115: 546–553.
55. Shin JY, Jung HJ, Moon A. Molecular markers in sex differences in cancer. *Toxicol Res* 2019; 35: 331–341.
56. Sakaguchi S, Goto H, Hanibuchi M, Otsuka S, Ogino H, Kakiuchi S, Uehara H, Yano S, Nishioka Y, Sone S. Gender difference in bone metastasis of human small cell lung cancer, SBC-5 cells in natural killer-cell depleted severe combined immunodeficient mice. *Clin Exp Metastasis* 2010; 27: 351–359.
57. Sun T, Warrington NM, Rubin JB. Why does Jack, and not Jill, break his crown? Sex disparity in brain tumors. *Biol Sex Differ* 2012; 3: 3.
58. Falk S, Uldall M, Appel C, Ding M, Heegaard AM. Influence of sex differences on the progression of cancer-induced bone pain. *Anticancer Res* 2013; 33: 1963–1969.
59. Romero-Reyes M, Salvemini D. Cancer and orofacial pain. *Med Oral Patol Oral Cir Bucal* 2016; 21: e665–e671.
60. Benoliel R, Epstein J, Eliav E, Jurevic R, Elad S. Orofacial pain in cancer: part I – mechanisms. *J Dent Res* 2007; 86: 491–505.
61. Diener KM. Bisphosphonates for controlling pain from metastatic bone disease. *Am J Health Syst Pharm* 1996; 53: 1917–1927.
62. Mantyh PW, Clohisy DR, Koltzenburg M, Hunt SP. Molecular mechanisms of cancer pain. *Nat Rev Cancer* 2002; 2: 201–209.
63. Fujita M, Andoh T, Ohashi K, Akira A, Saiki I, Kuraishi Y. Roles of kinin B1 and B2 receptors in skin cancer pain produced by orthotopic melanoma inoculation in mice. *Eur J Pain* 2010; 14: 588–594.
64. Robinson PP, Boissonade FM, Loescher AR, Smith KG, Yates JM, Elcock C, Bird EV, Davies SL, Smith PL, Vora AR. Peripheral mechanisms for the initiation of pain following trigeminal nerve injury. *J Orofac Pain* 2004; 18: 287–292.
65. Kitagawa J, Takeda M, Suzuki I, Kadoi J, Tsuboi Y, Honda K, Matsumoto S, Nakagawa H, Tanabe A, Iwata K. Mechanisms involved in modulation of trigeminal primary afferent activity in rats with peripheral mononeuropathy. *Eur J Neurosci* 2006; 24: 1976–1986.
66. Viviano M, Donati D, Lorenzini G. Metastatic carcinoma presenting as neuralgia involving the trigeminal nerve. *J Can Dent Assoc* 2012; 77: c32.
67. Menezes JD, Cappellari PF, Capelari MM, Gonçalves PZ, Toledo GL, Toledo Filho JL, Sales-Peres A, Marzola C. Mandibular metastasis of adenocarcinoma from prostate cancer: case report according to epidemiology and current

- therapeutical trends of the advanced prostate cancer. *J Appl Oral Sci* 2013; 21: 490–495.
68. Thalakoti S, Patil VV, Damodaram S, Vause CV, Langford LE, Freeman SE, Durham PL. Neuron-glia signaling in trigeminal ganglion: implications for migraine pathology. *Headache* 2007; 47: 1008–1023.
 69. Boada MD, Martin TJ, Peters CM, Hayashida K, Harris MH, Houle TT, Boyden ES, Eisenach JC, Ririe DG. Fast-conducting mechanoreceptors contribute to withdrawal behavior in normal and nerve injured rats. *Pain* 2014; 155: 2646–2655.
 70. Boada MD, Martin TJ, Ririe DG. Nerve injury induced activation of fast-conducting high threshold mechanoreceptors predicts non-reflexive pain related behavior. *Neurosci Lett* 2016; 632: 44–49.
 71. Boada MD, Martin TJ, Parker R, Houle TT, Eisenach JC, Ririe DG. Recovery from nerve injury induced behavioral hypersensitivity in rats parallels resolution of abnormal primary sensory afferent signaling. *Pain* 2020; 161: 949–959.
 72. Scheff NN, Ye Y, Bhattacharya A, MacRae J, Hickman DN, Sharma AK, Dolan JC, Schmidt BL. Tumor necrosis factor alpha secreted from oral squamous cell carcinoma contributes to cancer pain and associated inflammation. *Pain* 2017; 158: 2396–2409.
 73. Zhu J, Miao XR, Tao KM, Zhu H, Liu ZY, Yu DW, Chen QB, Qiu HB, Lu ZJ. Trypsin-protease activated receptor-2 signaling contributes to pancreatic cancer pain. *Oncotarget* 2017; 8: 61810–61823.
 74. Inoue K, Tsuda M. Microglia and neuropathic pain. *Glia* 2009; 57: 1469–1479.
 75. Pinho-Ribeiro FA, Verri WA Jr, Chiu IM. Nociceptor sensory neuron-immune interactions in pain and inflammation. *Trends Immunol* 2017; 38: 5–19.
 76. Kuol N, Stojanovska L, Apostolopoulos V, Nurgali K. Role of the nervous system in cancer metastasis. *J Exp Clin Cancer Res* 2018; 37:5.